Joint International Topical Meeting on Mathematics & Computation and Supercomputing in Nuclear Applications (M&C + SNA 2007)
Monterey, California, April 15-19, 2007, on CD-ROM, American Nuclear Society, LaGrange Park, IL (2007)

HIGH PERFORMANCE FVFE MULTIDOMAIN NUMERICAL METHOD TO PERFORM RADIONUCLIDES TRANSPORT CALCULATIONS

M. Dymitrowska*, M. Bourgeois, and G. Mathieu
Institut de Radioprotection et de Sûreté Nucléaire
DSU/SSD/BECS
BP 17
92262 Fontenay-aux-Roses, France
magdalena.dymitrowska@irsn.fr

ABSTRACT

This paper aims at describing numerical methods developed within the Melodie code to perform 3D saturated flow and transport calculations in the framework of radioactive waste geological repository. The diffusive type terms are discretised by a standard finite-element method and the convective term is treated with a Godunov-type finite-volume approach. The simulation domain is meshed using a structured tetrahedral mesh generator, which fulfils the Delaunay and cotangent criteria. In order to deal with a high number of computational nodes and different refinement levels, a domain decomposition strategy has been developed. As an example of the relevance of this numerical method we present calculations performed on the French "spent fuel / iron canisters / clay" concept designed by ANDRA in the frame of the feasibility study of a radioactive waste geological disposal. The analysis aims at assessing the influence of transfer properties of three radionuclides ^{79}Se, ^{94}Nb and ^{129}I which differ in terms of solubility, sorption and chemical speciation.

Key Words: radionuclides transport, radioactive waste geological repository, finite volume-finite element method, domain decomposition

1. INTRODUCTION

In order to support its technical appraisal of nuclear operator files, IRSN performs independent research and studies. IRSN develops in particular MELODIE code to model radionuclides migration from radioactive waste repository to the ground surface. This type of computational modeling is a quite challenging task due to the presence of strong heterogeneities (physical, chemical, hydrogeological) and because of very different geometrical scales (from cm to km) which are dealt with simultaneously. Although, using an appropriate numerical approach (FVFE and domain decomposition), it is possible, as shown in the present paper, to simulate at once the whole repository with the highly contrasted transport regimes from pure diffusion up to the marked advective process. The results of a sensibility analysis on chemical forms of two radionuclides (RN) are presented in section 3 and 4. They illustrate how this numerical method was used for a practical modeling case within the nuclear safety context in the frame of the 6th European Framework Project NF-Pro [7].

* author to whom the correspondence should be addressed

2. MELODIE CODE

The MELODIE software is the numerical tool developed by IRSN in collaboration with Paris School of Mines and University of Pau to model the integrated transport of RN from waste repositories to the ground surface.

2.1. Conceptual model

The geological formation is represented by an equivalent heterogeneous porous medium. All solid materials are considered as saturated with water and the RN are present in solution as tracers, e.g. they do not modify the water properties. The physical processes taken into account are the following:

- saturated flow following Darcy's law:

$$S\frac{\partial H}{\partial t} - \nabla.(K\nabla H) + q = 0 \quad (1)$$

  where $U = -K\nabla H$ is the Darcy velocity [m.year^{-1}], H is the hydraulic head [m] : $H = \frac{p}{g\rho} + z$ with p being the pressure [Pa], g gravity acceleration [m.s^{-2}], and ρ is the water density [kg.m^{-3}], K is the permeability tensor [m.year^{-1}], S is the specific storage [m^{-1}] and q is the flow source term [year^{-1}].
- advective/diffusive transport of the radionuclide accounting for radioactive decay and chains with retardation of transport through instantaneous sorption:

$$\omega R\frac{\partial A}{\partial t} - \nabla.(D\nabla A - AU) + Q - \lambda R\omega A = 0 \quad (2)$$

  Where A is the activity field [Bq.m^{-3}] of RN (directly proportional to the molar concentration), ω is the porosity, R is the retardation factor, λ is the decay constant [year^{-1}], Q is the source term [Bq.m^{-3}.year^{-1}], and D is the diffusion-dispersion tensor of the form :

$$D = (\alpha_T|U| + \omega d)I + (\alpha_L - \alpha_T)\frac{\vec{U}\otimes\vec{U}}{|U|} \quad (3)$$

  Where α_L and α_T are the longitudinal and transversal (with respect the direction of flow) dispersivities [m], d is the molecular diffusion constant [m^2.year^{-1}] and ⊗ designs tensor sum.
- solubility limit of a RN : $A(\vec{r},t) \le A^{\max}$, where $A^{\max}$ is the maximal volume activity of the RN. This condition achieved at the source term node by the means of Dirichlet condition and elsewhere with a redistribution procedure between precipitated (immobile) and solubilized (mobile) fractions of the RN.

Both D and K tensors can be anisotropic and all other material dependent parameters can be heterogeneous and radionuclide dependent.

2.2 Numerical method

The initial design of the MELODIE code was based on finite element (FE) method for numerical approximation of flow (1) and transport equations (2). The FE method, used intensively to solve parabolic and elliptical problems, is not satisfying for dealing with possible discontinuities in solutions and with convection terms, especially when the convection is dominating. To improve the accuracy and the reliability of calculations a method called FVFE - Finite Volume Finite Element [1] - is adapted in the code without major modification in terms of numerical implementation. Its principle is to use a *Galerkin* development for the unknowns in time and for diffusion type terms. The convection term is processed by a finite volume method using a Godunov P_1 scheme with a possible extension to the second order by using TVD slope limiters. Attention is paid to locally conservative numeric schemes, providing solutions that satisfy the principle of the maximum. FVFE method operates on triangular (2D) or tetrahedral (3D) meshes and requires constructing a dual mesh. This dual mesh can be based on centers of gravity (FVFECG) or on circumcenters (FVFECC) connected with centers of the edges (2D) or with the gravity centers of triangular faces (3D), Fig. 1. The second construction is feasible under the restriction of the acute mesh angles on the boundary of the calculation field. Note that the elementary contributions, relating to the diffusion, convection and time terms, are calculated on the dual mesh (on its boundary C_j) included in a primal meshing element to guarantee local conservativity of the method (flow velocity and material characteristics are constant in elements of the primal mesh T_k). We will further focus on the 3D FVFECG variant since this is the approach used in our sensitivity analysis example from section 4. We discuss only the discretization of the transport equation as it will also apply in identical way to the flow equation (which contains a diffusion type term only).

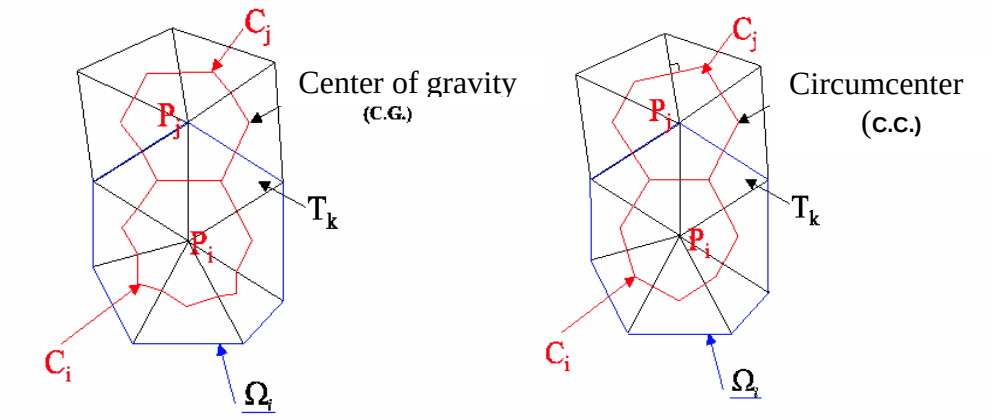

Figure 1 : Dual meshes for FVFE method : gravity center (left), circumcenter (right)

2.2.1 FVFE center of gravity scheme in 3D

By T_h is noted a triangulation of the Ω study field in $\mathbb{R}^3$, and by $k \in \mathbb{R}_+^*$ the time step. $t_n = nk$ is established for $n \in N$. For a mesh node i, the control volume noted C_i is constructed by the center of gravity method.

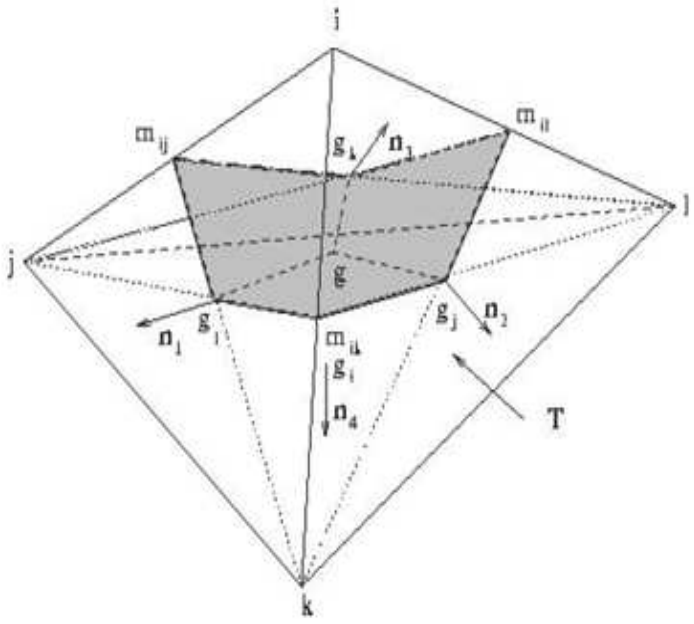

Figure 2 : Dual mesh included in T, constructed by the CG method

It is obtained by a meeting of the dual sub-meshes (see Fig. 2) included in the elements surrounding the node *i*. The principle of the FVGECG method is to integrate the flow and transport equations in a control volume C_i, apply Green's formula to bring the diffusive and convective flows together, to use a *Godunov*-type scheme for the approximation of the convective term and use a *Galerkin* P_1 development for the unknowns. Given the theorem of divergence, the integration of the equations (3) with C_i gives:

$$\int_{C_i} \omega \frac{\partial A}{\partial t} dx - \int_{\partial C_i} \left(D\nabla A - AU \right) \cdot n d\sigma + \int_{C_i} Q dx = 0. \tag{4}$$

Subsequently, the three faces $(gg_k m_{ij} g_l)$, $(gg_l m_{ik} g_j)$ and $(gg_j m_{il} g_k)$ will be noted respectively by σ_1, σ_2 and σ_3, their unit normals facing outwards by $\bar{n}_1, \bar{n}_2$ and $\bar{n}_3$ and the sub-faces of T - $(im_{ij} g_l m_{ik})$, $(im_{ik} g_j m_{il})$ and $(im_{ij} g_k m_{il})$ - by Σ_1, Σ_2 et Σ_3 and their unit normals facing outwards by $\mathbf{n_1}$, $\mathbf{n_2}$ and $\mathbf{n_3}$.

2.2.2 Approximation of the term over time

The temporal approximation of the term over time in (4) is achieved with a Euler scheme, using a *Galerkin* P_1 development of A:

$$\int_{C_i} \omega \frac{\partial A}{\partial t} dx \approx \sum_{T;P \in T} \sum_{j} \frac{A_j^{n+1} - A_j^n}{k} \int_{C_i \cap T} \omega N_j dx, \tag{5}$$

Performing mass lumping (5) implies

$$\int_{C_i} \omega \frac{\partial A}{\partial t} dx \approx \frac{A_i^{n+1} - A_j^n}{k} \omega_T \left| C_i \right|, \tag{6}$$

where ω_T designates an approximation of ω on T. In the 3D version of MELODIE, mass lumping is used by default. In the 2D version, a choice may be made between mass lumping and the approximation of the temporal term using a Gauss quadrature formula.

2.2.3 Approximation of the diffusive term

The approximation of the diffusive flux in (4) by the FVFECG method is based on an implicit scheme:

$$-\int_{\partial C_i} D\nabla A \cdot n d\sigma \approx -\sum_{T;P_i\in T}\int_{\partial C_i\cap T} D_T \nabla A^{n+1}\cdot n d\sigma, \tag{7}$$

where $\mathbf{D}_T$ is an approximation of the diffusion-dispersion tensor on the element T.and by

$$\alpha_{ij}^{diff}(T) = -\int_{\partial C_i\cap T} D_T \nabla N_j \cdot n d\sigma \tag{8}$$

the elementary diffusive term. It can be shown that $a_{ij}^{diff}(T)$ calculated by the FVFECG method is equal to the finite element diffusive term :

$$a_{ij}^{diff}(T) = \frac{|ikl|}{3|T|}\frac{|jkl|}{3|T|}(D_T n_2, n_4)|T| \tag{9}$$

2.2.4 Approximation of the convective term

The classical choice is available in MELODIE to treat the convective flux. The discretisation is based on *Godunov*-type scheme with the time dependence treated via a mixing scheme than can be varied from implicit to explicit. For the sake of simplicity in this section the time index n will therefore be omitted. We establish first:

$$\int_{\partial C_i} AU\cdot n d\sigma \approx \sum_{T;i\in T}\left(|\sigma_1|A|\sigma_1 U_T\cdot\bar{n}_1 + |\sigma_2|A|\sigma_2 U_T\cdot\bar{n}_2 + |\sigma_3|A|\sigma_3 U_T\cdot\bar{n}_3\right) \tag{10}$$

On the dual face σ_1 separating the nodes i and j, $c|\ \sigma_1 U_T\cdot\bar{n}_1$ is approached as follows:

$$A|U_T\cdot\bar{n}_1 \approx A_i(U_T\cdot\bar{n}_1)^+ + A_j(U_T\cdot\bar{n}_1)^- \tag{11}$$

where $r^+ = \max(0, r)$ and $r^- = \min(0, r)$ for $r\in\mathbb{R}$..

$$a_{ij}^{conv}(T) = |\sigma_1|(U_T\cdot\bar{n}_1)^-, a_{ii}^{conv}(T) = |\sigma_1|(U_T\cdot\bar{n}_1)^+ + |\sigma_2|(U_T\cdot\bar{n}_2)^+ + |\sigma_3|(U_T\cdot\bar{n}_3)^+ \tag{12}$$

It is clear that $A|\sigma_1$ is approached by taking account of the flow direction.

We note by

$$a_{ij}^{conv}(T) = |\sigma_1|(U_T\cdot\bar{n}_1)^-, a_{ii}^{conv}(T) = |\sigma_1|(U_T\cdot\bar{n}_1)^+ + |\sigma_2|(U_T\cdot\bar{n}_2)^+ + |\sigma_3|(U_T\cdot\bar{n}_3)^+ \tag{13}$$

the elementary convective terms. Therefore (11) implies:

$$\begin{aligned}\int_{\partial C_i} AU\cdot n d\sigma &\approx \sum_{T;i\in T} a_{ii}^{conv}(T)A_i + a_{ij}^{conv}(T)A_j + a_{ik}^{conv}(T)A_k + a_{il}^{conv}(T)A_l \\ &= \sum_{T;i\in T}\left(a_{ii}^{conv}(T)A_i + \sum_{j\in V_T(i)} a_{ij}^{conv}(T)A_j\right)\end{aligned} \tag{14}$$

2.2.5 Approximation of Darcy velocity field

The *Darcy* velocity field **U** is expressed as a function of the hydraulic head *H* from (1). As *H* is approached using a *Galerkin P1* development, the approximation of **U** is constant on each element *T*; it will be noted by $\mathbf{U}_T$. The result, taking (1) into account is

$$U_T = -\sum_{j \in >T} H_j K_T \nabla N_j . \tag{15}$$

For *j* designating a node in *T* as illustrated in Figure 1, we have $\nabla N_j = -\frac{|ikl|}{3|T|} n_2$ and therefore $\mathbf{U}_T$, by noting here by F_j the face opposite to the node *j* in *T* and $\mathbf{n}_j$ the unit normal at F_j facing outwards, as follows :

$$U_T = \frac{1}{3|T|} \sum_{j \in T} H_j |F_j| K_T n_j . \tag{16}$$

2.2.6 Time schemes with FVFE method

FVFE implicit scheme is unconditionally stable provided the *Delaunay*-type mesh admissibility conditions are respected. The linear system with a non-symmetrical matrix is resolved at each time step by calling a conjugate bi-gradient solver. In FVFE semi-implicit scheme the convective term is treated explicitly and approached by a *Godunov*-type scheme. In addition to a *Delaunay* condition for the mesh, this type of scheme requires a CFL condition to ensure its stability. In our case it can be shown that the time step $\delta\Delta t$ should be smaller than CFL value given by :

$$CFL_2 = \frac{\min\{\omega_T |C_i|; i, T; i \in T\}}{\max\{|U_{C_i} \cdot n|_{\max}; i\} \max\{|\partial C_i|; i\}} \tag{17}$$

The semi-implicit scheme results, at each time step, in a symmetrical linear system, which MELODIE solves with a conjugate gradient solver.

2.2.7 Optimality criteria for CG dual mesh

This construction has the advantage of keeping the CG centre noted here as ***g*** inside the tetrahedron *T*. Under the hypothesis that the tensor **D** is equivalent to a scalar; **D** = *D***I**, the elementary contribution $a_{ij}^{diff}(T)$ is given by:

$$a_{ij}^{diff}(T) = -\frac{1}{6} D_T |kl| \cot an(\theta_{kl}) \tag{18}$$

Note by ε_{ij} all the edges opposite (*ij*), belonging to tetrahedrons with (*ij*) as a common edge. For $e \in \varepsilon_{ij}$, the tetrahedron with edges *e* and (*ij*) is noted T_e and the dihedral angle in T_e relating to *e* is noted θe. The extradiagonal global diffusive coefficient a_{ij}^{diff} is calculated as follows:

$$a_{ij}^{diff} = -\frac{1}{6} \sum_{e \in \varepsilon_{ij}} D_{T_e} |e| \cot an(\theta_e). \tag{19}$$

Therefore if the following condition is checked:

$$\sum_{e \in \varepsilon_{ij}} D_{T_e} |e| \cot an(\theta_e) \geq 0, \tag{20}$$

it can be said that the mesh is optimal. Such a condition, called cotangent criterion, has a no local character and is in principle difficult to fulfill on unstructured meshes.

2.2.8 Mesh generator

In general it is not possible to mesh arbitrary volume geometry with a non structured tetrahedral mesh fulfilling all optimality criteria [2]. We have developed a structured tetrahedral mesh generator which fulfills the cotangent criteria (20), the Delaunay criteria and is fully self-centered, e.g. each tetrahedron contains its circumcenter (optimality criterion required for the FVFECC method). It is also possible to refine the mesh simultaneously in two dimensions without loosing the above mentioned properties. The basic element of the mash is a cube (or rectangular paralleliped) that can be split in two ways into prisms which also have two possible divisions into 3 tetrahedra (it is also possible to split a cube into 5 tetrahedra but this division doesn't fulfill the cotangent criterion and they are not self-centered). A special organization in 2D plane is necessary, see Fig.3.

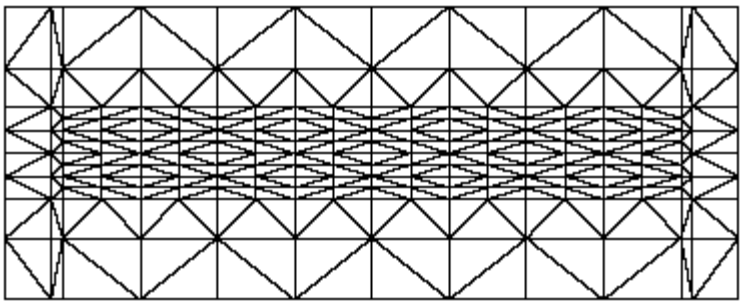

Figure 3 : 2D mesh organisation for domains 5 to10 from fig.6. The number of refined elements must be a multiple of 4 and a special size layer must be placed between refined and initial size elements.

2.3 Parallel virtual machine architecture.

We are often dealing with simulations of structures with characteristic sizes varying by several orders of magnitude. Therefore we encounter the problem of choosing the right mesh size. It can not be too large (because of the Peclèt and Fourier criteria) neither too small since the number of nodes and elements that can be used depends on the RAM that can be allocated to the processor. Currently simulations with more than 1 500 000 of elements become problematic, mostly because of the pre and post-processing limitations. In order to overcome this difficulty we have adopted a domain decomposition strategy with Dirichlet-Dirichlet coupling. With the use of PVM library it has been possible to parallelize the computations for use on a cluster of processors.

The simulation domain is split into overlapping meshes for independent calculations. To maintain the continuity of the solution the domains exchange information about the overlaying zone, Fig.4. This example features two domains (1 and 2) exchanging information (hydraulic head and activity). The fields values calculated in domain 1 on node "a" is used as a boundary condition for domain 2. Following the same process, on the next calculation step, the values obtained for node "b" in domain 2

will serve as BC for domain 1. This coupling may be done over one or several elements layers (rows). It has to be noted that one of the domains has to be solved before the other one.

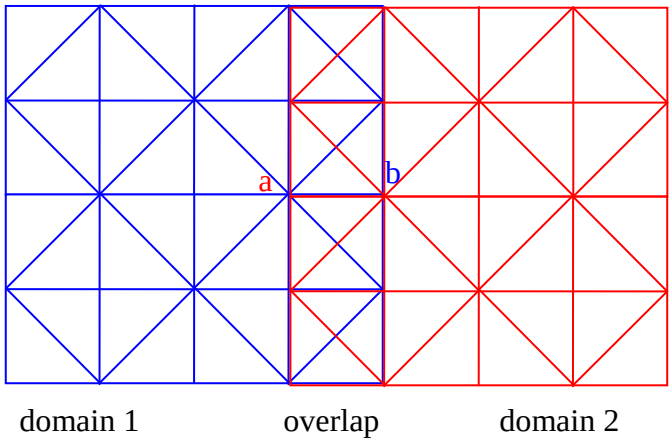

Figure 4 : Principle of domain decomposition with the overlap thickness of one layer.

This means that not all domain calculations can be carried out simultaneously. Parallelisation is only possible for domains that are not shearing with each other an overlap zone. A sequence of priority has to be carefully defined in order to optimise the parallelization.

For each time step of resolution of the global problem a new iteration process is added in order to assure the continuity between individual domain calculations. The convergence is reached when in *all* domains the maximal relative error calculated between two successive iterations on overlapping zones nodes is smaller than a prescribed value, typically 10^{-6}. This means that all domains perform the same number of iterations. It has been observed that the convergence is obtained quicker if the thickness of the overlapping zone is larger. However in practice a. large overlapping zone rapidly decreases the memory gain obtained with the domain decomposition and also complicates notably the calculations pre-processing stage.

2.4 Validation of the FVFE method

In order to validate the numerical settings, several tests on flow and transport cases has been performed. We present briefly hereafter only one example of 2D transport case. A continuous point source term of activity placed in an uniform flow field. The test has been done with the Peclèt number Pe= 1.1. In Fig. 5 the numerical FVFE solution on the line passing through the source and parallel to the flow direction is shown against the analytical solution for a given time step. The associated relative and absolute errors are plotted on the following figure. Close to the source the relative error is of the order of 0.01, while it increases near to both domains borders due to imposed boundary conditions (no diffusive flow though inflow and outflow boundary).

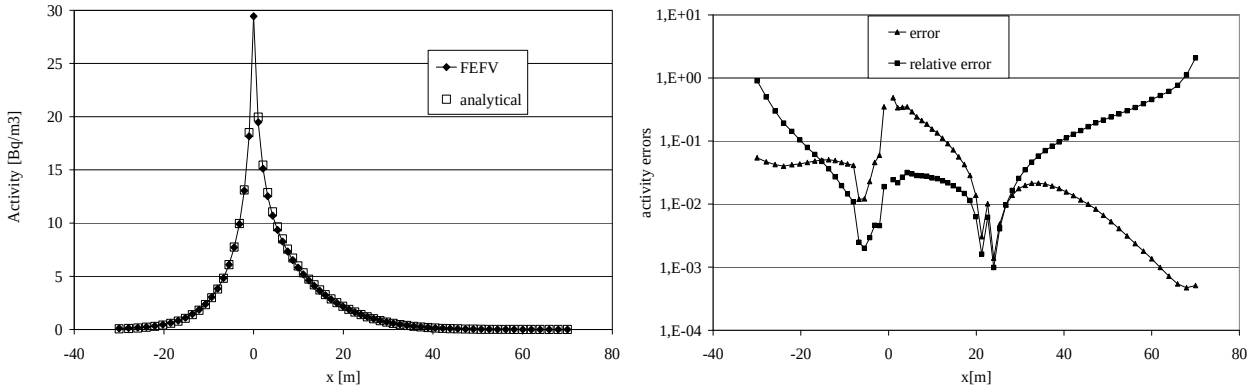

Figure 5 A sample test case for the FVFE method. Activity profile passing through the continuous point source (left) and the corresponding errors (right).

3. DESCRIPTION OF A REAL LIFE CASE FOR SENSITIVITY ANALYSIS

The purpose of the following calculations is to simulate the migration of radionuclides from disposal cells thought the repository system at a realistic scale.

3.1 Description of the repository system

The calculation domain, modeled in 3D, represents a part of the geological layer of Callovo-Oxfordian (COX) clay and contains a simplified representation of main components of the repository. The repository structure consists of a vertical access shaft connecting the repository level with the ground surface, a long horizontal drift (main drift in Fig.6), a handling drift connecting the main drift to the disposal cell, 6 disposal cells and engineered barriers (seals and plugs). The shaft is closed in its upper part by a seal and its lower part is filled by concrete. A seal in the vicinity of the shaft closes the main drift. A seal supported by concrete plugs also closes the handling drift. The remaining space in the shaft and the drifts contains a backfill. Three spent fuel containers are placed in each disposal cell. The space between the waste packages and the disposal cell wall is filled with bentonite clay. Each disposal cell is closed by a bentonite plug and a concrete reinforcement. The excavation-damaged zone (EDZ) surrounding the repository system depends on the excavation's diameter. Its thickness is taken equal to the half of the excavation's diameter. Most of the dimensions of the repository components are based on Andra concept, except of the lengths of different drifts which are arbitrary chosen [5]. The vertical shaft though the host rock is 65.5 meters deep and 12 meters large. The main drift is 727.85 meters long and 7 meters large. The handling drift is 177.5 meters long and 7 meters large. Each disposal cell is 40 meters long and 3 meters large. The seal of the shaft is 30 meters long. Concrete filling at the base of the shaft is 50 meters long. The main and handling drift seals are each 44 meters long. The concrete plugs of the handling drift are each 7 meters long. The disposal cell seals are each 3 meters long and the concrete filling is 7 meters long. The engineered barrier is 30 meters long and 3 meters large. And the waste canisters are only represented as punctual activity sources. In the original concept all excavations have circular section which is replaced in our calculations by a square one.

The domain is 786.1 meters long, 268 meters wide and 129 meters thick.

The global mesh is composed of 4 052 538 tetrahedral elements and 732 864 nodes distributed in 10 embedded meshes.

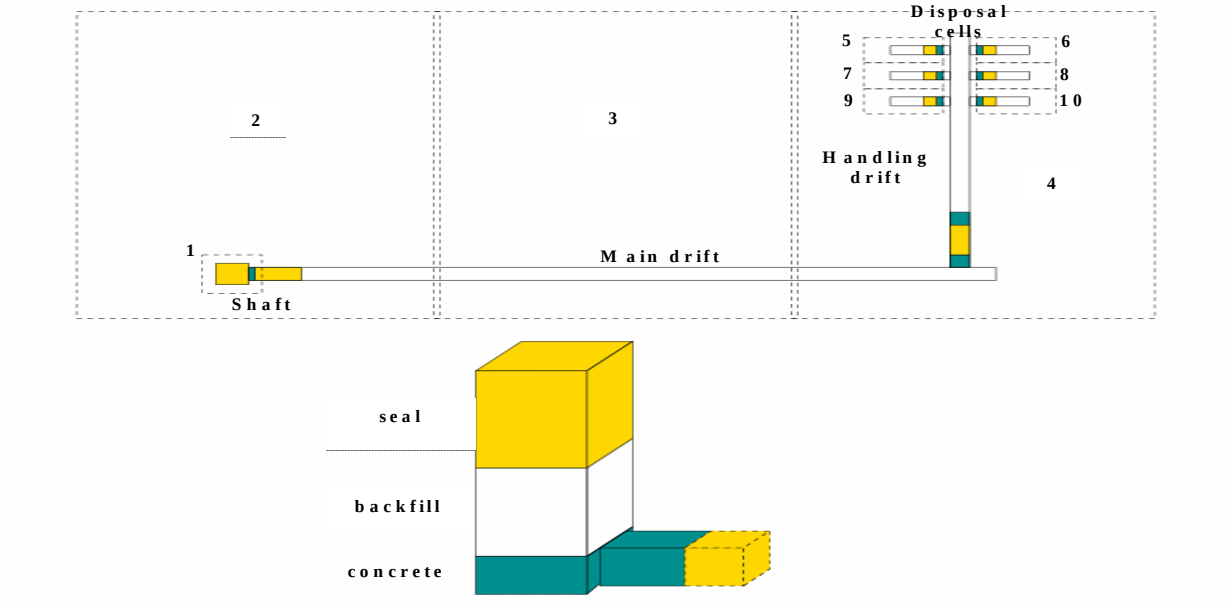

Figure 6 : Repository system and the shaft - 10 embedded meshes

The hydraulic boundary conditions applied are 350 meters hydraulic head at the bottom of the COX formation and 305 meters hydraulic head at the top boundary of the COX.

3.2 Data

We model the migration of the following radionuclides presenting contrasted radiological and chemical proprties: ^{129}I (non sorbed and soluble), ^{79}Se (non sorbed and non soluble) and ^{94}Nb (sorbed and non soluble). The source terms accounts for the release of radionuclides from various parts of a waste package (labile fraction, UO_2 matrix release and metallic parts corrosion). We model the degradation process of the UO_2 matrix as dominated by alpha radiolysis on the UO_2 surface. The inventory, degradation rates and percentage of radionuclides mass per canister were provided by ANDRA [4]. The resulting source term is presented in Fig.7.

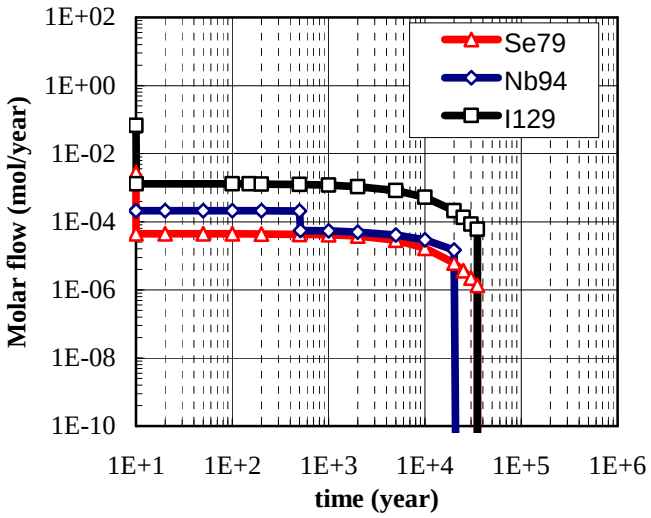

Figure 7. Radionuclides source term for reference case

Table I presents the main transport parameter values for the reference calculations. The parameters' values are from [5] or based on an educated guess. As the chemical forms of radionuclides are supposed to be anionic the anionic exclusion in clay pores causes low diffusion accessible porosity in all clayey materials. The permeability tensor in the Callovo-Oxfordian clay has two eigenvalues: the horizontal one is about one hundred times higher than the vertical one. Sorption processes including adsorption, chemical adsorption, absorption and ion exchange are described by the retardation factor R (2). The solubility limits and the retardation factors are summarized in Table II.

Table I. Transport parameter values for all model components.

	Callovo-Oxfordian	EDZ	Bentonite (seal)	Concrete	Backfill
Permeability (m/y)	$1.58\ 10^{-5}$* $1.58\ 10^{-6}$	$1.58\ 10^{-1}$	$3.15\ 10^{-4}$	$3.15\ 10^{+1}$	$3.15\ 10^{+1}$
Kinematic porosity (%)	9	9	18	30	40
Effective diffusion coefficient (m²/y)	$1.58\ 10^{-4}$	$3.15\ 10^{-4}$	$1.58\ 10^{-4}$	$1.89\ 10^{-2}$	-
Effective diffusion porosity for anions (%)	5	15	5	30	-
Pore diffusion coefficient (m²/y)	$3.15\ 10^{-3}$	$2.10\ 10^{-3}$	$3.15\ 10^{-3}$	$6.3\ 10^{-2}$	$3.15\ 10^{-2}$

Table II. Retardation factors and solubility limits for the of the radionuclides.

	Callovo-Oxfordian	EDZ	Bentonite (seal)	Concrete	Backfill	Solubility limit [mol/m^3]
^{129}I	1	1	1	8	1	soluble
^{79}Se	1	1	1	1	1	$5\ 10^{-7}$
^{94}Nb	53 400	53 400	350 000	70 000	1	$2\ 10^{-4}$

4. RESULTS OF THE SENSITIVITY CALCULATIONS

In order to quantify the radionuclides migration we use the synthetic transport indicators corresponding to the molar flux of a given element at the interfaces between different model components.

- at the outer boundary of the bentonite plug between the disposal tunnel and the drift (Φ_1)
- around the drift at the interface between EDZ and host rock (Φ_2);

4.1 Definition of the scenario.

A “reference” scenario is established in order to reproduce the expected performance of the components, particularly of drift seals.

4.1.1 Flow calculations.

According to measured hydraulic heads on Meuse/Haute Marne site, the vertical hydraulic head gradient is chosen equal to 0.2 m/m through the Callovo-Oxfordian. The upward velocity of the water flow calculated in the host rock is very low (0.4 μm/year) as a result of the very low permeability of the Callovo-Oxfordian (longitudinal permeability = $1.58\ 10^{-5}$ m/year and orthogonal permeability = $1.58\ 10^{-6}$ m/year). As a consequence the dominant regime of transfer through the homogeneous host rock is diffusion. The water flow velocities in the disposal cells are low (10^{-6} m/year) because of dead-end design, and diffusion is the dominant transfer regime. In the backfilled drift, velocities in the vicinity of the shaft ($5\ 10^{-2}$ m/year) are higher than close to the disposal cells ($5\ 10^{-5}$ m/year); the transfer regime is advective/diffusive close to the cells and advective in the vicinity of the shaft.

4.1.2 Transport calculations.

For ^{79}Se, the major part of mass released in the engineered barrier is precipitated. ^{94}Nb is characterized by strong sorption properties in clayey components and ^{129}I is non-sorbed and soluble in the clayey components. For ^{129}I and ^{79}Se the molar flows through the engineer barrier (Φ_2) into the host rock are one order of magnitude higher than the molar flows through the plug (Φ_1) into the drift (Fig. 8). The most significant part of the released mass (from 80 to 90 %) moves towards the host rock because the

transfer regime is diffusive in the disposal cells and the contact area between the cells and the clayey formation is important. For ^{94}Nb, molar flow is low (10^{-9} mol/year in TableIII) at the interface between EDZ and host rock (Φ_2) and is negligible through the plug (10^{-17} mol/year) because of the high sorption in the clayey materials. Sorption increases highly the transfer time through the clayey components with respect of the half-life of ^{94}Nb (20 300 years), as a consequence its mass is strongly reduced by radioactive decay. The results at the interface between EDZ and host rock (Φ_2) show that the gap between the molar flows of ^{129}I and ^{79}Se is of 4 orders of magnitude for the near field because of the control by solubility limit in the vicinity of the canisters for ^{79}Se. As expected the solute moves by diffusion through the host rock to the top and at the bottom of the Callovo-Oxfordian.

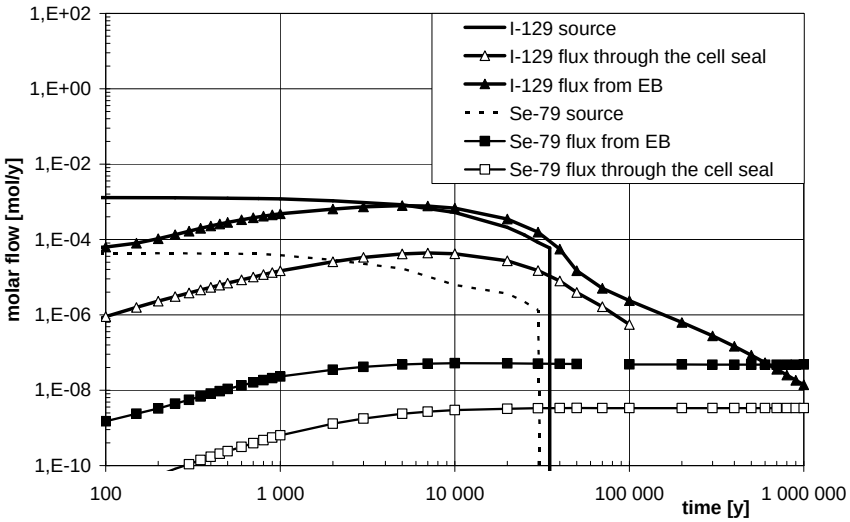

Figure 8 Molar flows through the disposal cell seal (Φ1) and through the engineered barrier (Φ2)

Table III. Maximum molar flow in mol/year.

^{129}I	Φ_1= 4.4 10^{-05} Φ_2= 8.0 10^{-04}
^{79}Se	Φ_1= 3.4 10^{-09} Φ_2= 5.2 10^{-08}
^{94}Nb	Φ_1= 1.8 10^{-17} Φ_2= 1.1 10^{-09}

4.2 Modified chemical forms of ^{79}Se and ^{94}Nb

Since the chemical form of ^{79}Se and ^{94}Nb are uncertain we repeat the previous calculations neglectiong the anionic exclusion in EDZ and bentonite. For both radionuclides, pore diffusion values are increased by one order of magnitude and the solubility limit values for selenium and niobium are taken higher (10^{-2} mol/m^3 except in concrete and backfill where niobium is taken soluble). This will allow us to test the stability of our numerical method against various transport controlling phenomena (sorption,

solubility and radioactive decay). The transport and chemical parameters are summarized in Table II [4][6].

The transfer time for niobium is decreased proportionally to the retardation factor; the loss of mass due to the radioactive decay during the transfer time is also smaller. This is in particular visible in Φ_1 values since transfer distance from the source is much longer then for Φ_2(Fig. 9 and Table IV). When ^{94}Nb is considered as a non-sorbed radionuclide, molar flows Φ_1 and Φ_2 are in the same order of magnitude as ^{129}I molar flows, because fluxes from the waste are of the same order of magnitude.

In this sensitivity case the ^{79}Se solubility limit is too high to control release rate as it does in previous calculations (Fig. 9). When controlled by its solubility ^{79}Se release reaches a plateau and continues for a long time after total degradation of the waste matrix due to the high quantity of precipitated mass which acts as an additional source term. On the contrary, when ^{79}Se is considered as a soluble and non-sorbed radionuclide, values of molar flows Φ_1 and Φ_2 increase by a factor 1 000 in the same order of magnitude as molar flows released from the canisters. In this case, because of the high pore diffusion value (because anionic exclusion is not taken into account), the influence of the instantaneous release fraction is visible after a few tens of years.

Table IV. Maximum molar flow in mol/year from a disposal cell.

	reference	increased diffusion + high solubility	
		no sorption of Nb	sorption of Nb divided by 100
^{94}Nb	Φ_1= 1.8 10^{-17} Φ_2= 1.1 10^{-09}	Φ_1= 1.3 10^{-05} Φ_2= 1.4 10^{-04}	Φ_1= 1.6 10^{-09} Φ_2= 1.7 10^{-07}
^{79}Se	Φ_1= 3,4 10^{-09} Φ_2= 5.2 10^{-08}	Φ_1= 6,9 10^{-06} Φ_2= 9.3 10^{-05}	

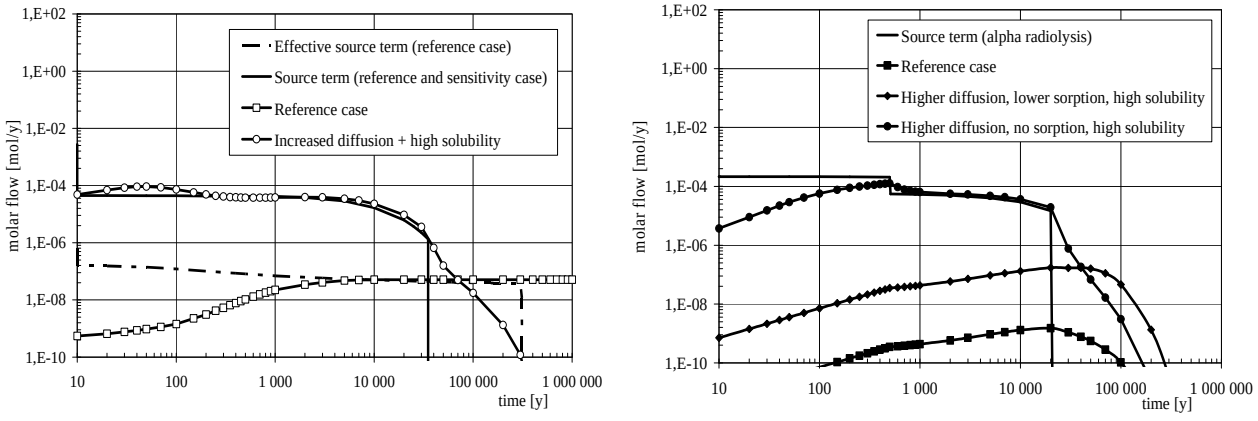

Figure 9 Molar flows of Nb(right) and Se(left) through the engineered barrier – modified chemical forms

5. CONCLUSIONS

We have presented here an efficient finite element-finite volume method for solving the equations of flow and convection-diffusion transport in saturated porous media. The procedure has been implemented in 3D on regular tetrahedral meshes. The method converges and fulfills the local maximum principle on highly heterogeneous (10^7 factor between the permeability values, 10^5 on retardation factors) and non-isotropic media and allows for a simple domain Dirichlet-Dirichlet decomposition. We performed sensitivity calculations on meshes of several millions of elements and obtained coherent results allowing theirs quantitative analysis. Since no negative activities (concentrations) appeared it is possible to use this code as a transport modulus for geochemical simulations.

ACKNOWLEDGEMENTS

The sensitivity analysis has been performed in the frame of the NF-Pro European Union project.

REFERENCES

1. M. Putti and C. Cordes, *Finite element approximation of the diffusion operator on tetrahedra*, SIAM J. Sci. Comput., 19 (1998), pp. 1154--1168.
2. M.Křižek, J.Pradlova, *Nonobtuse Tetrahedral Partitions*, Numerical Methods for Partial Differential Equations, Volume 16, Issue 3 , Pages 327 – 334, 2000
3. EU. NF-PRO. *Phenomenological Description. Reference Concept Spent Fuel and HLW-Iron Canister-Granite*. Deliverable D5.1.1. Part 2. Final version, June 30th 2005.
4. IRSN - *Avis de l'Institut de radioprotection et de sûreté nucléaire sur le Dossier 2005 Argile-Rapport DSU n°106*, 2005.
5. ANDRA , *Dossier 2005 Argile – Tome - Architecture et gestion du stockage géologique* , 2005.
6. IRSN, *Modeling approach for safety of high activity waste disposal*, International Symposium NUCEF2005, Tokai-mura, Ibaraki-ken, Japan, 2005.
7. EC, Bentonite *barriers in integrated performance assessment (BENIPA). Final Report*, EUR 21023, 2004.